MACHINE LEARNING APPLIED TO SENTINEL-2 AND LANDSAT-8 MULTISPECTRAL AND MEDIUM-RESOLUTION SATELLITE IMAGERY FOR THE DETECTION OF RICE PRODUCTION AREAS IN NGANJUK, EAST JAVA, INDONESIA

Terry Devara Tri Saadi[1], Arie Wahyu Wijayanto[2]*

[1,2] Department of Computational Statistics, Politeknik Statistika STIS, Jakarta, Indonesia

*e-mail: ariewahyu@stis.ac.id

Received: 5 February 2021; Revised: 26 March 2021; Approved: 28 May 2021

Abstract. Statistics Indonesia (BPS) has been introducing the use of Area Sampling Frame (ASF) surveys from 2018 to estimate rice production areas, although the process continues to suffer from the high costs of human and other resources. To support this type of conventional field survey, a more scalable and inexpensive approach using publicly-available remote sensing data, for example from the Sentinel-2 and Landsat-8 satellites, has been explored. In this research, we compare the performance gain from Sentinel-2 and Landsat-8 images using a multiple composite-index enriched machine learning classifier to detect rice production areas located in Nganjuk, East Java, Indonesia as a case study area. We build a detection model from a set of machine learning classifiers, Decision Tree (CART), Support Vector Machine, Logistic Regression, Ensemble Bagging Methods (Random Forest and Extra Trees), and Ensemble Boosting Methods (AdaBoost and XGBoost). The composite indices consist of the NDVI and EVI for agricultural and forest areas, NDWI for water and cloud, and NDBI, NDTI, and BSI for built-up areas, fallows, and asphalt-based roads. Validated by k-fold cross-validation, Sentinel-2 and Landsat-8 achieved F1-scores of 0.930 and 0.919 respectively at the scale of 30 meters per pixel. Using a 10 meter resolution per pixel for the Sentinel-2 imagery showed an increased F1-score of up to 0.971. Our evaluation shows that the higher spatial resolution imagery of Sentinel-2 achieves a better prediction, not only performance-wise, but also as a better representation of actual conditions.

Keywords: *multispectral remote sensing, medium-resolution optic, machine learning, rice detection*

1 INTRODUCTION

Rice is the major staple food for Indonesian people. However, according to an official publication by Statistics Indonesia (BPS), the production area of rice in 2019 was 10.68 million hectares, a decrease of 700.05 thousand hectares (6.15%) compared to 2018. Moreover, production in 2019 is predicted to be around 54.60 million tons of dry unhusked paddy, or 6.60 million tons (7.76%) less than 2018 (BPS-Statistics Indonesia, 2020). Therefore, to achieve national food security and the second of the Sustainable Development Goals (SDGs,) food monitoring has become crucial.

BPS has conducted food monitoring by utilising the Area Sampling Frame (ASF), known as “Kerangka Sampel Area” (KSA) in the official language, which is performed using spot field surveys designated as sample segments (BPS-Statistics Indonesia, 2015). Nevertheless, KSA still has a major disadvantage as the level of resources needed is considerable.

On the other hand, remote sensing data can be obtained easily and could be applied to all kinds of fields (Triscowati, Sartono, Kurnia, Domiri, & Wijayanto, 2019, 2020; Wijayanto, Triscowati, & Marsuhandi, 2020). Some examples of remote sensing utilisation are land cover classification (Ienco, Gaetano, Dupaquier,

& Maurel, 2017); poverty prediction (Jean, Burke, Xie, Davis, Lobell, & Ermon, 2016); burned area mapping (Fitriana, Suwarsono, Kusratmoko, & Supriatna, 2020); and crop classification (Kussul, Lemoine, Gallego, Skakun, Lavreniuk, & Shelestov, 2016).

In contrast to conventional field surveys, employing publicly available remote sensing data could lead to a more scalable, inexpensive, and real-time method. While studies on the application of Random Forest on multi-temporal Landsat 8 data have been conducted (Triscowati et al., 2019, 2020), the data and method used are still limited to Landsat 8 and Random Forest respectively. In this study, several machine learning methods were employed on Sentinel-2 and Landsat-8 imagery to detect rice-production areas in order to provide a more affordable option for food monitoring. The study focus is on investigating the effect of different satellite image resolutions and model classifiers in improving detection accuracy.

2 MATERIALS AND METHODOLOGY

2.1 Location and Data

This study was conducted in Nganjuk in East Java, a landlocked regency located at a latitude of 7.6°S and longitude of 111.9333°E, as shown in Figure 2-1. An area of approximately 1.182,64 km^2, 404,586 hectares, is covered by rice fields, with a production of 232,413 tons in 2018 (BPS-Statistics Indonesia, 2019). Although other regencies have higher rice production, the land in this area has certain distinctive characteristics, with both flat and mountainous regions. Even though it is landlocked, a relatively large river flows across the regency, and it is one of the regencies crossed by the Trans-Java highway.

In this research, 2A-level-processed Sentinel-2 images acquired on 14 March 2020 and Landsat-8 tier 1 surface reflectance acquired on 16 March 2020 were used to perform the analysis and evaluation (Figure 2-1). The sample used for each class, as well as the training data samples, are shown in Table 2-1 and Figure 2-2.

Table 2.1: Number of pixels in sample data

	S2 (10)	S2 (30)	L8
Built-up	16276	2663	2663
Water	4904	825	825
Agriculture	13364	1826	1826
Fallow	18335	2653	2653
Forest	17891	2302	2302
Asphalt	3138	796	796
Cloud	14847	1907	1639

Sentinel-2 is a multi-spectral wide-swath, medium-resolution imaging mission aimed at supporting Copernicus Land Monitoring studies involving the monitoring of vegetation, soil, and water cover, beyond the observation of aqueducts and coastal areas. With four bands at 10 meter, six bands at 20 meter, and three bands at 60 meter spatial resolution, the Sentinel-2 Multispectral Instrument (MSI) samples 13 spectral bands with a 5 day revisit period (European Space Agency, n.d.). The Sentinel-2 images used in this research were at a 10 meter resolution/S2(10) and rescaled 30 meter resolution/S2(30).

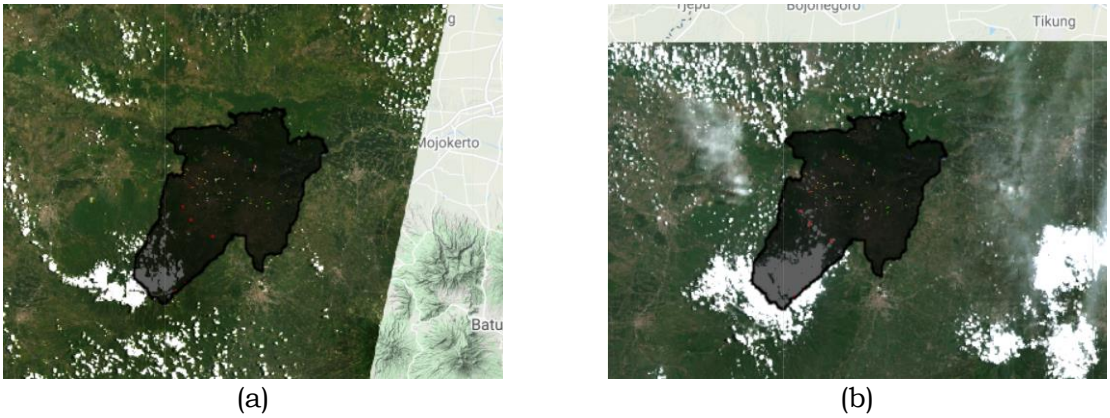

Figure 2-1: (a) Landsat-8 image used in the study shown in true colour; (b) Sentinel-2 image used in the study shown in true colour. The black masking shows the border of the Nganjuk regency used as the study area.

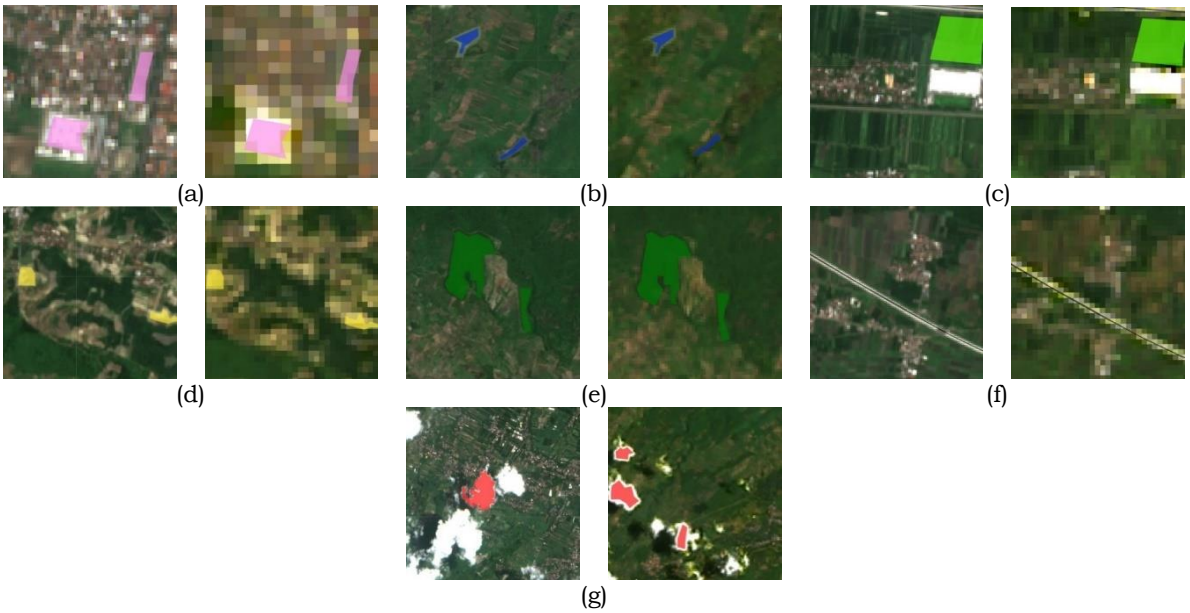

Figure 2-2: True colour imagery of each class, left-hand side from Sentinel-2, and right-hand side from Landsat-8. The classes from top to bottom are (a) built-up area, (b) water surface, (c) rice-field, (d) fallow, (e) forest, (f) highway, and (g) cloud coverages

Landsat 8 Surface Reflectance (SR) Science Products are generated from specialised software called Land Surface Reflectance Code (LaSRC). It also has improved geometric accuracy by implementing Sentinel 2 Global Reference Image (GRI) into Landsat 8 OLI ground control points. Landsat 8 SR is also equipped with seven visible bands and two thermal bands with a 30 meter spatial resolution and a 16 day revisit period (USGS, 2019). The features of each satellite can be seen in Table 2-2.

The basic features used in this research are the blue, green, and red bands, together with the near-infrared (NIR), shortwave infrared 1 (SWIR1), and shortwave infrared 2 (SWIR2) bands. Several indices were also used, namely the Normalized Difference Vegetation Index (NDVI) and Enhanced Vegetation Index (EVI), which were used to help differentiate between field and forest. In addition, the Normalized Difference Water Index (NDWI) was employed to distinguish between water surfaces and cloud, and the Normalized Difference Built-up Index (NDBI), Normalized Difference Tillage Index (NDTI), and Bare Soil Index (BSI) were used to help

differentiate between fallows, built-up areas, and highways. The formulas related to these indices are:

$$NDVI = \frac{NIR - RED}{NIR + RED} \quad (2\text{-}1)$$

$$NDWI = \frac{GREEN - NIR}{GREEN + NIR} \quad (2\text{-}2)$$

$$NDBI = \frac{SWIR1 - NIR}{SWIR1 + NIR} \quad (2\text{-}3)$$

$$NDTI = \frac{SWIR1 - SWIR2}{SWIR1 + SWIR2} \quad (2\text{-}4)$$

Two formulas can be used to count EVI, the first original formula being:

$$EVI = 2.5 * \frac{NIR - RED}{NIR + 6 * RED - 7.5 * BLUE + 1} \quad (2\text{-}5)$$

The second formula does not use the blue channel and is called EVI2:

$$EVI2 = 2.5 * \frac{NIR - RED}{NIR + 2.4 * RED + 1} \quad (2\text{-}6)$$

2.2 Decision Tree (CART)

The term Classification and Regression Tree (CART) (Breiman et al., 1984) refers to decision trees for predictive modeling problems using both classification tree and regression tree analysis, creating a decision tree in which each node makes a binary decision to break up one class from another.

2.3 Support Vector Machine

Support Vector Machine (SVM) (Drucker et al., 1997) is a classifier that produces nonlinear bounds by devising a linear boundary in a big, altered version of the feature space.

Table 2-2: Sentinel-2 MSI and Landsat 8 OLI instrument spectral band specification.

Sentinel-2 MSI Level-2A			
Band	**Description**	**Resolution (m)**	**Wavelength (nm)**
B1	Aerosols	60	443.9 (S2A) / 442.3 (S2B)
B2	Blue	10	496.6 (S2A) / 492.1 (S2B)
B3	Green	10	560 (S2A) / 559 (S2B)
B4	Red	10	664.5 (S2A) / 665 (S2B)
B5	Red Edge 1	20	703.9 (S2A) / 703.8 (S2B)
B6	Red Edge 2	20	740.2 (S2A) / 739.1 (S2B)
B7	Red Edge 3	20	782.5 (S2A) / 779.7 (S2B)
B8	NIR	10	835.1 (S2A) / 833 (S2B)
B8A	Red Edge 4	20	864.8 (S2A) / 864 (S2B)
B9	Water vapor	60	945 (S2A) / 943.2 (S2B)
B10	Cirrus	60	1373.5 (S2A) / 1376.9 (S2B)
B11	SWIR 1	20	1613.7 (S2A) / 1610.4 (S2B)
B12	SWIR 2	20	2202.4 (S2A) / 2185.7 (S2B)

Landsat-8 Surface Reflectance Tier 1			
Band	**Description**	**Resolution (m)**	**Wavelength (µm)**
B1	Ultra blue	30	0.435-0.451
B2	Blue	30	0.452-0.512
B3	Green	30	0.533-0.590
B4	Red	30	0.636-0.673
B5	NIR	30	0.851-0.879
B6	SWIR 1	30	1.566-1.651
B7	SWIR 2	30	2.107-2.294
B10	Brightness temperature	30	10.60-11.19
B11	Brightness temperature	30	11.50-12.51

2.4 Ensemble Bagging Methods

Bagging, or bootstrap, aggregation is an approach for decreasing the variance of an estimated prediction function. In high-variance, low-bias programs such as trees, bagging appears to perform particularly well. For regression, the same regression trees were fitted several times to bootstrap sample versions of the training data and the outcome averaged. For classification, a vote was cast by panels of trees for the predicted class.

2.4.1 Random Forests

Random forests (Breiman, 2001) are a modified version of bagging; they assemble a sizeable library of de-correlated trees and then average them. Although very similar to bagging in performance in relation to many problems, random forests are easier to train and tune. This has led to their popularity and implementation in a variety of packages.

2.4.2 Extra Trees

Extremely randomized trees (Geurts et al., 2006), also known as extra trees, fundamentally involve the vigourous randomisation of both attribute and cut-point selection, while splitting a tree node. In extreme cases, randomised trees with independent architectures from the output values of the learning sample are constructed. Problem-specific tuning of randomisation strength can be made using the appropriate choice of parameter.

2.5 Ensemble Boosting Methods

The incitation of boosting aimed to create a very large “committee” by combining the results of numerous “weak” classifiers. The boosting approach bears similarity to bagging and other committee-based methods. A weak classifier is one with an error rate barely better than stray speculation. By consecutively applying this weak classification algorithm to continually altered versions of the data, a string of weak classifiers is created. Through a weighted majority vote, the predictions of these weak classifiers produce the final prediction (Hastie et al., 2013). In this study, the two most popular ensemble boosting methods, AdaBoost and XGBoost, were used as classifiers.

2.6 Classification Framework

The classification framework for this study is described below.

Step 1: Connect Google Colab to Google Earth Engine and Google Drive, and download Sentinel-2 and Landsat 8 imagery of the study area. Since these satellites have different revisit times, the imagery used must be taken on dates close to each other. There is also a high chance that the imagery on the following date will have too much cloud cover to be usable. Since Sentinel-2 has other bands not available on Landsat-8, the bands used in this research will be limited to those available to both satellites.

Step 2: Extract the pixel value of the area to be used as the sample. For Sentinel-2, the images will also be rescaled to 30m x 30m, the same resolution as Landsat-8, to allow a comparison of the classification results with the same scale and to observe whether the resolution will affect the classification results.

Step 3: Add a composite index for all the imagery.

Step 4: Perform classification of all the imagery. CART decision tree, CART decision tree with bagging, Random Forest, Extremely Randomized Trees, Logistic Regression, Linear SVM, AdaBoost decision tree, XGBoost tree, and linear were employed. For all classifiers in each imagery, perform k-fold cross-validation with k=10.

3 RESULTS AND DISCUSSION

3.1 Data Exploration

Based on the boxplot of each band on the seven classes, information about the extent to which each band differentiates the labels could be collected. It can be observed from Figures 3-1, 3-2, and 3-3 that although each band could distinguish a certain class quite well individually, other classes continue to show similar values. It can be seen that NDVI could distinguish between rice fields and forests, but its value for other classes is similar. On the other hand, NDBI could distinguish between built-up areas and fallows, while other classes showed little difference.

From further examination, it appears that even though NDBI could identify built-up areas and fallows from the rest of the class, it could not tell the differences between them. On the other hand, even though NDTI could not differentiate between built-up areas and highways, it had no problem in identifying the differences between the remaining classes. Hence, by combining these two composite indices, it was possible to discern built-up areas, fallows, and highways. Consequently, a classification model could be constructed by applying this logic to other bands in other classes.

Sentinel-2 10m

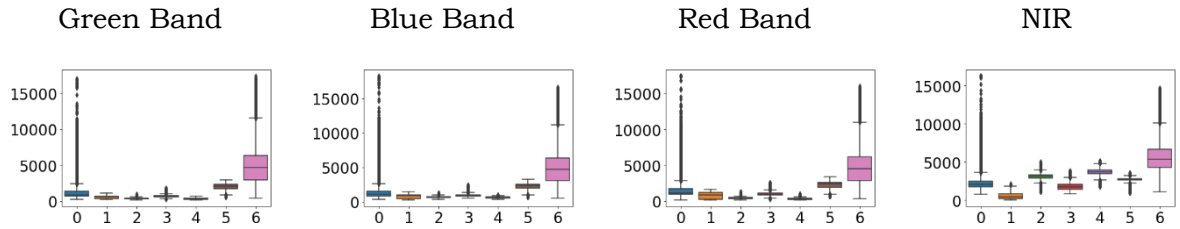

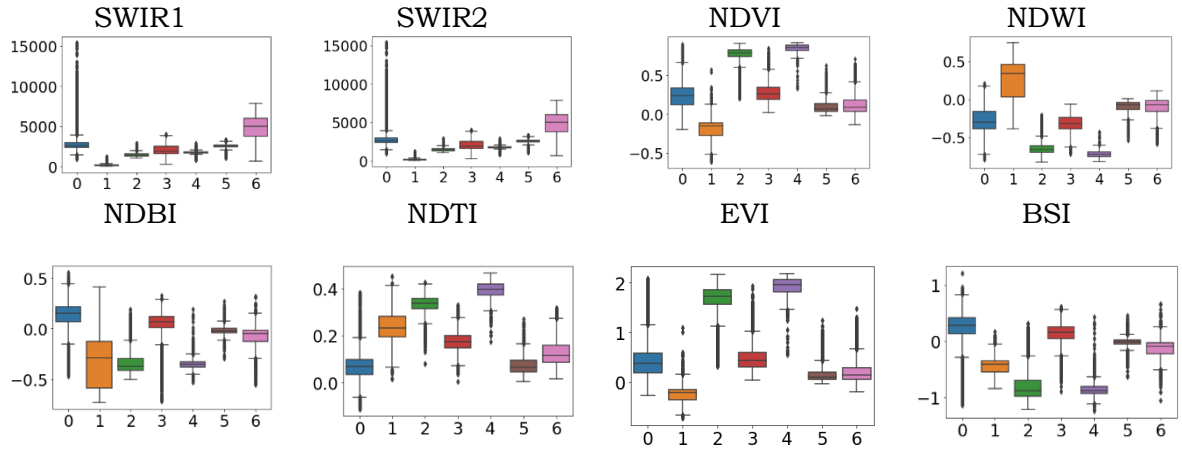

Figure 3-1: Distribution of bands and composite index values per class with Sentinel-2 10m resolution

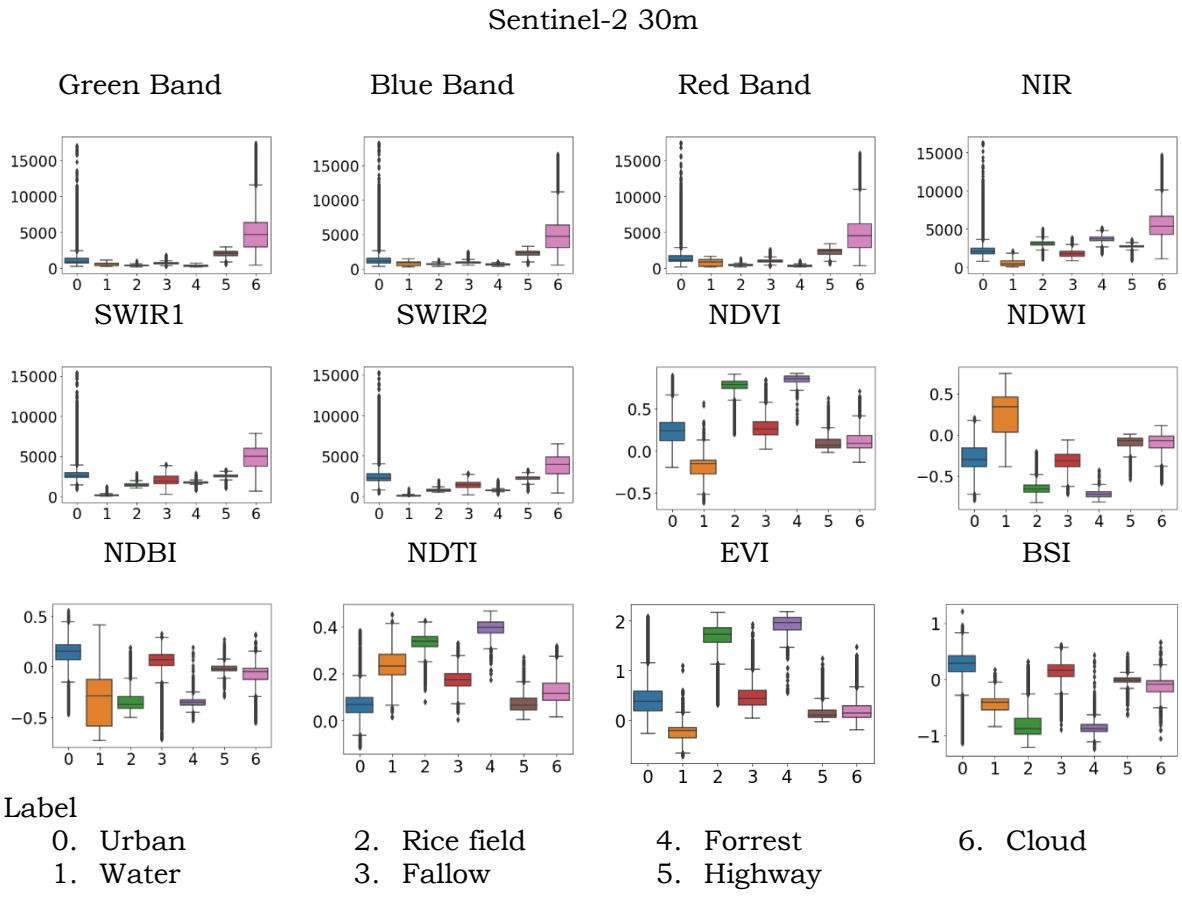

Figure 3-2: Distribution of bands and composite index values per class with Sentinel-2 30m resolution

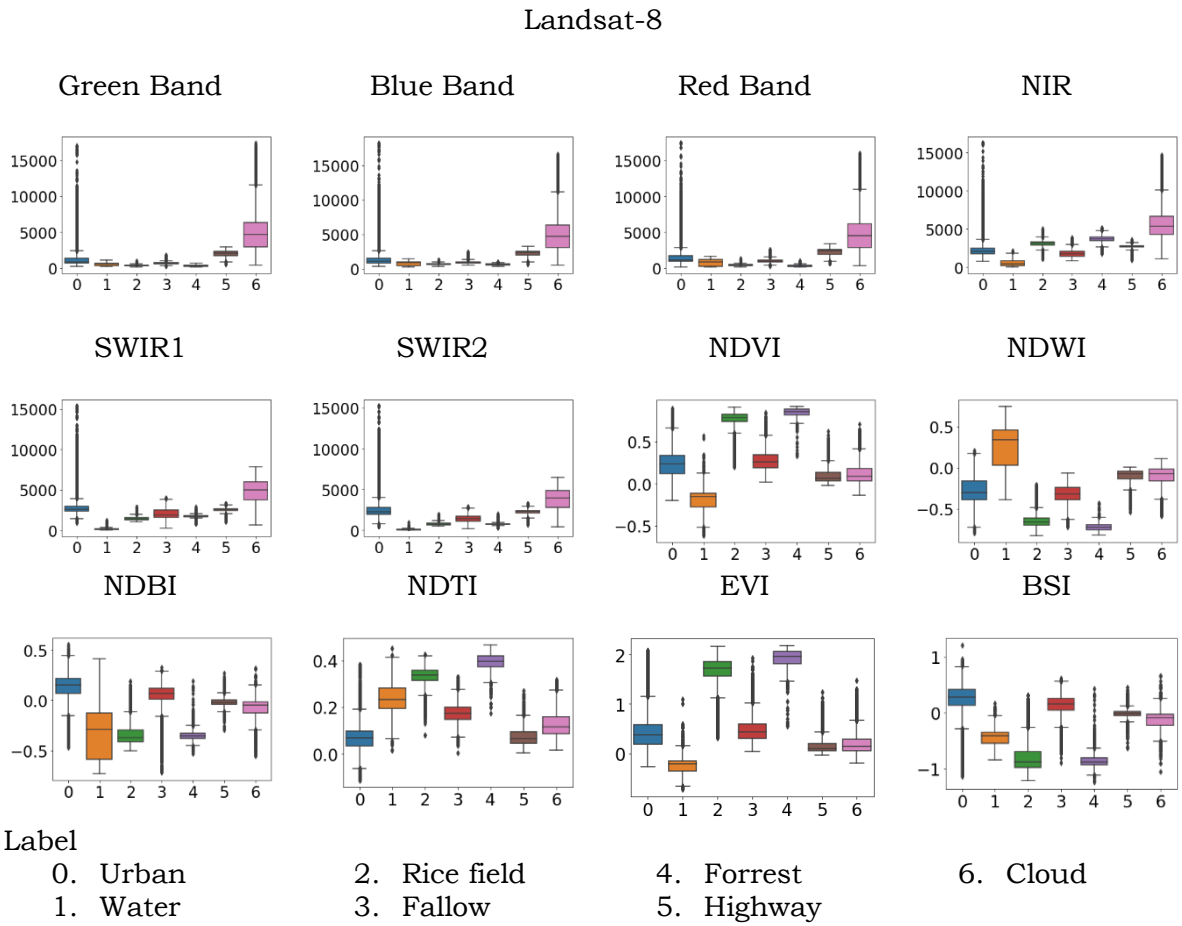

Figure 3-3: Distribution of bands and composite index values per class with Landsat-8

Table 3-1: 10-fold cross-validation results of all models with Sentinel-2 10m resolution, Sentinel-2 30m resolution, and Landsat-8 for combined classes.

Classification Model	F1-Score			Standard Deviation		
	S2 (10)	S2 (30)	L8	S2 (10)	S2 (30)	L8
Random Forest	0.971	0.930	0.919	0.002	0.006	0.007
Decision Tree	0.952	0.906	0.888	0.003	0.006	0.010
Decision Tree with Bagging	0.971	0.932	0.922	0.002	0.005	0.008
Extra Trees	0.968	0.927	0.915	0.002	0.005	0.008
Logistic Regression	0.942	0.919	0.911	0.003	0.005	0.008
Linear SVM	0.803	0.814	0.834	0.037	0.010	0.017
AdaBoost (Decision Tree)	0.954	0.932	0.929	0.014	0.006	0.005
XGBoost (gbtree)	0.948	0.907	0.912	0.003	0.006	0.007
XGBoost (gblinear)	0.673	0.622	0.641	0.006	0.017	0.013

3.2 Model Results

All the classification models used went through a grid search for hyperparameter tuning to optimise the results of each. A comparison of all the classification methods for all the images can be seen in Table 3-1. The values displayed are the result of performing 10-fold cross-validation, which means that the whole sample was split into ten partitions, nine of which were used as training data, and one as testing data. The training and testing process was then repeated ten times, with a different partition used as testing data. Based on

the table, the classification result for S2(10) is better than that for almost every other model. Classification of S2(30) and L8 did not show any significant difference.

In line with this result, resolutions make a great contribution to the classification results, since both the S2(30) and L8 results do not show a great difference, while some models yield better results for S2(30) and others have a better outcome for L8. This indicates that when performed at the same scale or resolution, the results from S2(30) and L8 do not show a significant difference.

Table 3-2 shows that using random forest classification for S2(10) yields a significantly better result compared to S2(30) and L8 for the detection of rice production areas. Despite having an acceptable recall, both S2(30) and L8 have inferior precision. While the model for S2(30) and L8 is good at recognizing rice fields based on the high recall value, the lower precision value describe that several other areas besides rice-field were predicted as rice-field. This could be quite problematic as it could lead to overestimation of rice production if areas which are not rice fields are identified as such. In this case, overestimation could be disastrous, because decision-makers would think that food stocks were sufficient when in fact they were not, which could lead to nationwide starvation.

Table 3-2: Precision, Recall, and F1-score of each class for each image using random forest classification

Class	Precision			Recall			F1-score		
	S2(10)	S2(30)	L8	S2(10)	S2(30)	L8	S2(10)	S2(30)	L8
Built-up	0.97	0.91	0.95	0.94	0.88	0.92	0.95	0.90	0.94
Water	1.00	0.97	0.98	1.00	0.94	0.95	1.00	0.95	0.96
Rice-field	0.95	0.83	0.87	0.97	0.92	0.92	0.96	0.88	0.89
Fallow	0.96	0.90	0.91	0.98	0.90	0.94	0.97	0.90	0.93
Forrest	0.99	0.97	0.99	0.99	0.97	0.95	0.99	0.97	0.97
Highway	0.90	0.85	0.90	0.88	0.80	0.83	0.89	0.83	0.86
Cloud	0.99	0.98	0.96	0.98	0.96	1.00	0.98	0.97	0.98

Table 3-3: Comparison of confusion matrix using random forest classification

S2(10)							
	0	1	2	3	4	5	6
0	1592	0	25	49	1	20	10
1	0	478	0	0	0	0	0
2	4	1	1306	14	17	0	0
3	22	0	14	1816	0	0	1
4	1	0	23	1	1744	0	0
5	13	0	0	14	0	257	9
6	12	0	2	3	0	7	1420

S2(30)							
	0	1	2	3	4	5	6
0	241	0	8	16	0	7	1
1	0	73	3	2	0	0	0
2	4	0	176	5	6	0	0
3	5	2	15	234	1	2	1
4	0	0	6	0	216	0	0
5	9	0	2	4	0	64	1
6	5	0	1	0	0	2	186

L8							
	0	1	2	3	4	5	6
0	256	0	6	5	0	4	6
1	1	89	2	2	0	0	0
2	5	0	162	9	1	0	0
3	3	2	9	253	1	2	0
4	3	0	6	2	221	0	0
5	2	0	2	6	1	57	1
6	0	0	0	0	0	0	152

Table 3-4: Feature importance of random forest model

	S2 (10)	S2 (30)	L8
Blue	0.06387	0.06318	0.09400
Green	0.05761	0.05050	0.07327
Red	0.04344	0.04919	0.05385
NIR	0.09967	0.10329	0.07722
SWIR1	0.14596	0.14543	0.09278
SWIR2	0.11893	0.13152	0.10989
NDVI	0.06536	0.05647	0.06249
NDWI	0.05696	0.05398	0.04558
NDBI	0.04629	0.05845	0.06476

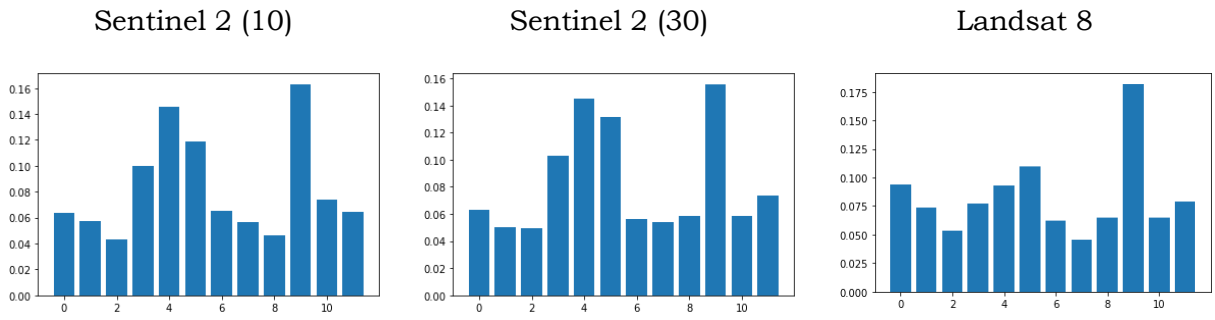

Figure 3-4: Feature importance plot of random forest model

From further examination of the confusion matrix from the previous classification (Table 3-3), it seems that the reason for the precision of S2(30) and L8 was from built-up land, fallow, and forest being predicted as rice fields. Because this problem does not appear in the S2(10) classification, it means that one of the possible reasons for this classification concerns the spatial resolution of the imagery.

The samples for the research were taken in a polygon which consisted of vectors; when those vectors were applied to pixels, then the area included in the polygons would vary according to the pixel size. With a higher spatial resolution image, this method did not pose a real problem, since the area did not change. However, with lower spatial resolution images, the area taken as samples would change dramatically, as the size of each pixel would be significantly larger. As a result, areas that were not intended to be included were taken as samples, which then affected the value of the bands or indices used. A simple example would be the use of Sentinel-2 images. The native spatial resolution of some of the Sentinel-2 bands is 10 meters per pixel; when this is rescaled to 30 meters per pixel, each new pixel contains nine of the original ones. The way Google Earth Engine handles this is by using the mean value of the native pixels as the value for the new ones (Google Developers, 2017).

Following this train of thought, there is a possibility that when the sample area is being taken using these polygons, some areas of other classes, specifically fallows, are taken as rice fields, and vice versa. This affects the value of the pixels included in the samples, leading to other classes being predicted as rice fields.

In addition, information about the contribution of each feature used by the Random Forest model can be seen in Table 3-4 and Figure 3-4. The scores suggest that for S2(10) and S2(30), Random Forest found NIR, SWIR1, SWIR2, and NDTI to be the most significant features. Although the other features made contributions, these were not as significant as these four features. L8, however, shows that NDTI makes the most significant contribution, while the other features do not contribute as much. One point to keep in mind is that the importance of this feature was not applied to one specific class, but to all the classes used in the model.

4 CONCLUSION

After conducting a detailed experiment by evaluating a wide range of powerful machine learning methods in relation to Landsat-8 and Sentinel-2, we selected both Random Forest and Decision Tree with Bagging on Sentinel 2 with 10 meters spatial resolution as the best performing machine learning classifier of satellite data for detecting rice production areas. The following conclusions can be drawn.

Using higher resolution imagery could lead to an increase in classification accuracy. Furthermore, the scope of the class used and the extent to which the classification is performed can also be increased. Although the aim of the study was to detect rice production areas, it also shows the possibility of differentiating between normal built-up areas and highways by using an even higher resolution image, showing not only highways, but also the regular streets that are too small for Sentinel-2 and Landsat-8. This could help in other fields of statistics.

Utilising polygons to collect sample data for training purposes could make the collection of large amounts of training data easier. One issue to be wary of is that the data collected using this method could be noisy or may not match the intended class.

Another issue to consider is that in this study, only bands available to both Sentinel-2 and Landsat-8 were used, although Sentinel-2 is equipped with several other bands, for example Red-Edge. According to Frampton, Dash, Watmough, & Milton (2013) and Delegido, Verrelst, Alonso, & Moreno, (2011), Sentinel-2 red B4 (665 nm) and the red-edge B5 (705 nm) bands give great correlations during estimation of the leaf area index and chlorophyll content. Therefore, by utilising these spectral bands, not only can better classification of rice fields be made, but also rice growth phases.

ACKNOWLEDGEMENTS

The authors would like to thank the journal editorial team and reviewer for providing suggestions for the manuscript.

AUTHOR CONTRIBUTIONS

TDTS & AWW conceptualized the research objectives. TDTS carried out the code writing, experimental simulations, analysis, visualization, and writing original draft preparation. AWW selected the methodology, supervised the project, review and editing the manuscript. All authors have read and agreed to the published version of the manuscript.

REFERENCES

BPS-Statistics Indonesia (2019). *Produksi Padi Setara Beras di Provinsi Jawa Timur Menurut Kabupaten/Kota (ha), 2018*

[Paddy Production Equivalent to Rice in East Java According to Regency/City (ha), 2018]. Retrieved January 18, 2021, from https://jatim.bps.go.id/statictable/2019/10/08/1584/produksi-padi-setara-beras-di-provinsi-jawa-timur-menurut-kabupaten-kota-ha-2018.html

BPS-Statistics Indonesia (2015). *Pedoman Pelaksanaan Uji Coba Sistem Kerangka Sampel Area [Area Sampling Frame Trials Implementation Guide]*. Retrieved January 18, 2021 from https://sirusa.bps.go.id/webadmin/pedoman/2016_3431_ped_Pedoman Pelaksanaan Uji Coba Kerangka Sampel Area (KSA)2015.pdf

BPS-Statistics Indonesia (2020). *Executive summary of paddy harvested area and production in Indonesia 2019*. Retrieved January 18, 2021 from https://www.bps.go.id/publication/2020/07/10/32247632fa792a2f3f28a644/ringkasan-eksekutif-luas-panen-dan-produksi-padi-di-indonesia-2019.html

Breiman, L. (2001). Random forests. *Machine Learning* **45,** 5–32

Breiman, L., Friedman, J. H., Olshen, R. A., & Stone, C. J. (1984). *Classification And Regression Trees*. Chapman and Hall/CRC incomplete

Delegido, J., Verrelst, J., Alonso, L., & Moreno, J. (2011). Evaluation of sentinel-2 red-edge bands for empirical estimation of green LAI and chlorophyll content. *Sensors*, *11*(7), 7063–7081.

Drucker, H., Surges, C. J. C., Kaufman, L., Smola, A., & Vapnik, V. (1997). Support vector regression machines. *Advances in Neural Information Processing Systems*, *January*, 155–161.

European Space Agency (n.d.). *User Guides - Sentinel-2 MSI - Overview - Sentinel Online - Sentinel*. Retrieved January 18, 2021, from https://sentinel.esa.int/web/sentinel/user-guides/sentinel-2-msi/overview

Fitriana, H. L., Suwarsono, S., Kusratmoko, E., & Supriatna, S. (2020). Mapping Burnt Areas Using the Semi-Automatic Object-Based Image Analysis Method. *International Journal of Remote Sensing and Earth Sciences (IJReSES)*, *17*(1), 57.

Frampton, W. J., Dash, J., Watmough, G., & Milton, E. J. (2013). Evaluating the capabilities of Sentinel-2 for quantitative estimation of biophysical variables in vegetation. *ISPRS Journal of Photogrammetry and Remote Sensing*, *82*, 83–92.

Geurts, P., Ernst, D., & Wehenkel, L. (2006). Extremely randomized trees. *Machine Learning*, *63*(1), 3–42.

Google Developers (2017). *Scale | Google Earth Engine | Google Developers*. https://developers.google.com/earth-engine/guides/scale

Hastie, T., Tibshirani, R., & Friedman, J. (2013). The Elements of Statistical Learning Data Mining, Inference, and Prediction. *Encyclopedia of Systems Biology*, 508–508.

Ienco, Di., Gaetano, R., Dupaquier, C., & Maurel, P. (2017). Land Cover Classification via Multitemporal Spatial Data by Deep Recurrent Neural Networks. *IEEE Geoscience and Remote Sensing Letters*, *14*(10), 1685–1689.

Jean, N., Burke, M., Xie, M., Davis, W. M., Lobell, D. B., & Ermon, S. (2016). Combining satellite imagery and machine learning to predict poverty. *Science*, *353*(6301), 790–794.

Kussul, N., Lemoine, G., Gallego, F. J., Skakun, S. V., Lavreniuk, M., & Shelestov, A. Y. (2016). Parcel-Based Crop Classification in Ukraine Using Landsat-8 Data and Sentinel-1A Data. *IEEE Journal of Selected Topics in Applied Earth Observations and Remote Sensing*, *9*(6), 2500–2508.

Triscowati, D. W., Sartono, B., Kurnia, A., Dirgahayu, D., & Wijayanto, A. W. (2020). Classification of Rice-Plant Growth Phase Using Supervised Random Forest Method Based on Landsat-8 Multitemporal Data. *International Journal of Remote Sensing and Earth Sciences (IJReSES)*, *16*(2), 187.

Triscowati, D. W., Sartono, B., Kurnia, A.,

Domiri, D. D., & Wijayanto, A. W. (2019). *Multitemporal remote sensing data for classification of food crops plant phase using supervised random forest*. *1131102*(November 2019), 10.

USGS (2019). *Landsat 8*. Retrieved January 18, 2021, from https://www.usgs.gov/core-science-systems/nli/landsat/landsat-8?qt-science_support_page_related_con=0#qt-science_support_page_related_con

Wijayanto, A. W., Triscowati, D. W., & Marsuhandi, A. H. (2020). Maize field area detection in East Java, Indonesia: An integrated multispectral remote sensing and machine learning approach. *ICITEE 2020 - Proceedings of the 12th International Conference on Information Technology and Electrical Engineering*, 168–173.